AIP Journal of Applied Physics

Low-temperature plasma-assisted growth of optically transparent, highly oriented nanocrystalline AlN

C. Mirpuri, S. Xu, J. D. Long, and K. Ostrikov

Citation: Journal of Applied Physics **101**, 024312 (2007); doi: 10.1063/1.2423224

View online: http://dx.doi.org/10.1063/1.2423224

View Table of Contents: http://scitation.aip.org/content/aip/journal/jap/101/2?ver=pdfcov

Published by the AIP Publishing

Low-temperature plasma-assisted growth of optically transparent, highly oriented nanocrystalline AlN

C. Mirpuri, S. Xu, and J. D. Long
Advanced Materials and Nanostructures Laboratory, Plasma Sources and Applications Center, NIE, Nanyang Technological University, 1 Nanyang Walk, Singapore 637616, Singapore

K. Ostrikov[a)]
Plasma Nanoscience@Complex Systems, School of Physics, The University of Sydney, Sydney NSW 2006, Australia

(Received 14 September 2006; accepted 1 November 2006; published online 19 January 2007)

Optically transparent, highly oriented nanocrystalline AlN(002) films have been synthesized using a hybrid plasma enhanced chemical vapor deposition and plasma-assisted radio frequency (rf) magnetron sputtering process in reactive $Ar+N_2$ and $Ar+N_2+H_2$ gas mixtures at a low Si(111)/glass substrate temperature of 350 °C. The process conditions, such as the sputtering pressure, rf power, substrate temperature, and N_2 concentration were optimized to achieve the desired structural, compositional, and optical characteristics. X-ray diffractometry reveals the formation of highly *c*-oriented AlN films at a sputtering pressure of 0.8 Pa. Field emission scanning electron microscopy suggests the uniform distribution of AlN grains over large surface areas and also the existence of highly oriented in the (002) direction columnar structures of a typical length ~100–500 nm with an aspect ratio of ~7–15. X-ray photoelectron and energy dispersive x-ray spectroscopy suggest that films deposited at a rf power of 400 W feature a chemically pure and near stoichiometric AlN. The bonding states of the AlN films have been confirmed by Raman and Fourier transform infrared spectroscopy showing strong *E*2 (high) and *E*1 transverse optical phonon modes. Hydrogenated AlN films feature an excellent optical transmittance of ~80% in the visible region of the spectrum, promising for advanced optical applications. © *2007 American Institute of Physics*.
[DOI: 10.1063/1.2423224]

I. INTRODUCTION

In the past decade, nitrides of group III semiconductors such as aluminum nitride (AlN), gallium nitride (GaN), and indium nitride , as well as their ternary and quaternary alloys (AlGaN and SiCAlN), have been the subject of intense research.[1] These compounds are promising candidates for their potential uses in optoelectronic devices in the ultraviolet/blue/green/yellow range for full color displays, semiconductor lasers, high-density information storage, and under water communication. Such materials are also used in high-temperature and high-power transistors which are needed for automobile engines, future advanced power distribution systems, electric vehicles, and avionics.[2] This is due to their large bond strengths and direct band gaps, the latter spanning a wide range of energies from 1.9 to 6.2 eV.[2,3] Among them, AlN is the most interesting compound with many outstanding physical properties, such as a direct band gap of 6.2 eV, high melting point of 3273 K, high thermal conductivity of 285 W/mK, and also a very high dielectric constant of 8.5.[3] AlN nanofilms are particularly useful as a buffer layer for the growth of compound semiconductors like GaN and AlGaN with a small lattice mismatch,[4] which is at the heart of advanced blue laser/light emitting diode technologies. In addition to that, an unusually high dielectric constant makes AlN a suitable substitute for SiO_2 in high-temperature metal-insulator-semiconductor integrated devices.[5]

For future nanodevice applications, AlN films are expected to be single crystalline with a smooth surface. Furthermore, a high-quality heteroepitaxy will be required to fully realize the outstanding potential of AlN in micro- and nanoelectronics. To fabricate device-grade AlN films, techniques such as vapor phase epitaxy,[6,7] molecular beam epitaxy,[4,7–9] chemical vapor deposition,[10] ion beam nitridation,[11] reactive sputtering,[12] and pulsed laser deposition[13] have been extensively used, with a different degree of success depending on specific process conditions. Even though advanced epitaxial techniques such as molecular beam epitaxy, chemical vapor deposition, and metallorganic chemical vapor deposition have been extensively used for the fabrication of lattice-matched nitrides of group III semiconductors, high process temperatures often result in a substantial thermal damage and film degradation. Moreover, the ability to synthesize highly oriented nanocrystalline films, which are of special interest as growth templates for zero- and one-dimensional quantum confinement structures [e.g., AlN serves as a lattice-matching buffer interlayer in the nanoassembly of SiC (Ref. 14) and $Al_xIn_{1-x}N$ (Ref. 15) quantum dot arrays and photoluminescent SiC-based nanoparticle films on Si(100)] (Ref. 16), still remains quite limited.

In order to synthesize highly oriented *c*-axis films,

[a)]Author to whom correspondence should be addressed; electronic mail: k.ostrikov@physics.usyd.edu.au

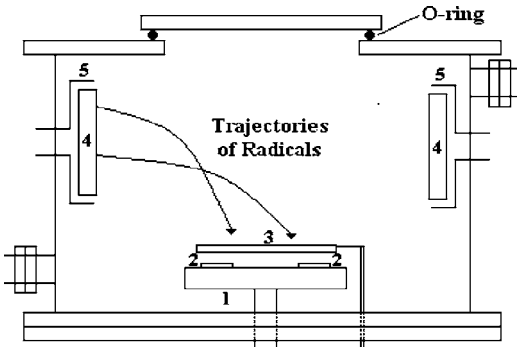

FIG. 1. Schematics of the experimental facility: (1) substrate holder; (2) substrates; (3) shutter; (4) sputtering target; and (5) target holder/magnetron electrode.

lower-temperature processes are required. Low temperature plasma-assisted reactive sputtering deposition is an excellent candidate owing to its apparent advantages in the ability to control the fluxes of numerous reactive species, the ease in handling and operation, and a relatively low cost. Recently, plasma-based processes have been successfully used for synthesizing various nanocrystalline films and aligned one- and two-dimensional nanostructures with crystallographic growth directions controlled by the plasma process conditions.[17–21] Likewise, plasma-aided radio frequency (rf) sputtering deposition provides a highly reliable and reproducible method of film growth[22] and as such should be particularly suitable for the synthesis of AlN nanofilms with a smooth surface and a negligible oxygen content, the latter still remaining a major concern for the many existing fabrication techniques.[5]

In this article, we report on the successful use of the plasma-assisted rf magnetron sputtering technique for the synthesis of optically transparent, highly oriented (002) nanocrystalline AlN films on Si(111) and glass substrates. The process conditions such as rf input power, substrate temperature, gas flow rates, and partial pressures have been optimized to obtain the desired structural, compositional, and optical properties of the AlN films critical for their envisaged applications.

II. EXPERIMENT

A schematic diagram of the AlN deposition chamber is shown in Fig. 1. The water-cooled stainless-steel-walled vacuum chamber with an inner diameter of 45 cm and height 30 cm is specially configured to meet the requirements of fine control of the product yield. A base pressure of 1 mPa was routinely achieved by a two-pump-system comprising a 5 l/s rotary pump and a 450 l/s turbomolecular pump. The base pressure was measured by using a vacuum multigauge system. An impedance-matching network was used to control the rf power input with less than 1% reflected power. It is different from conventional systems[23] where the target-to-substrate separation is generally smaller and reactions occur in the plasma bulk. Here, the sputtering of Al atoms and production of reactants occurs in the plasma near the high purity Al target of diameter 12 cm resting on a rf powered magnetron cathode. The magnetron electrode maximizes the film deposition rates due to the $\mathbf{E}\times\mathbf{B}$ drift, where $\mathbf{E}$ and $\mathbf{B}$ are the magnitudes of the electric and magnetic fields near the electrode.

TABLE I. Summary of process conditions.

Process parameter	Values
Base pressure	Below 10^{-3} Pa
N_2 flow rate	10–85 sccm
Ar flow rate	0–30 sccm
Substrate temperature	150–350 °C
rf power	200–400 W
Working gas pressure	0.4–1.4 Pa
Deposition time	0.5–3 h

Epitaxial growth of nitride semiconductors is commonly implemented on Si(111), Si(100), 3H/6H-SiC, α-Al_2O_3, or GaAs substrates.[2] In this work we use Si(111) because of the excellent match of its thermal expansion coefficient with that of AlN. To study the optical transmittance properties of AlN, polished glass substrates have been used. Before deposition, Si(111) and glass substrates were subjected to the Radio Corporation of America cleaning[24] process and immersed into 10% hydrofluoric acid for 30 s to remove a surface oxide layer. Before loading into the vacuum chamber, the substrates were blown dry by purified nitrogen. After the deposition chamber was evacuated to ~1 mPa, N_2, and/or Ar gas was introduced into the chamber and presputtered the target for 20 min, after which the shutter was opened. Table I summarizes the deposition parameters used to grow the AlN thin films.

A Siemens D5005 x-ray diffractometer (XRD) with an incident x-ray wavelength of 0.154 nm (Cu $K\alpha$ line) was used to analyze the crystallinity and crystallographic orientations of the AlN films. Surface morphology and cross-section were investigated by using a JEOL JSM-6700F field emission scanning electron microscope (SEM) coupled with an Oxford Instruments energy-dispersive x-ray (EDX) spectrometer. Chemical composition and bonding states were studied by x-ray photoelectron spectroscopy (XPS) using a 200-I-XL spectrometer equipped with a monochromatic Al $K\alpha$ (1486.6 eV) X-ray source. Raman and Fourier-transform infrared (FTIR) spectroscopy were used to investigate the phonon modes in the films. The Raman spectrum, with a spectral resolution of ~1.5 cm^{-1}, was obtained by using a Renishaw Micro-Raman System 1000 in a back-scattering mode at a wavelength of 514.5 nm. The infrared spectra were recorded by a Perkin Elmer Spectrum One FTIR spectrometer with a resolution of 4 cm^{-1}. Other details of the experimental facility, diagnostic instrumentation, auxiliary equipment, and characterization techniques can be found elsewhere.[19,22,25–27]

III. RESULTS AND DISCUSSION

The crystalline structure of all grown samples was characterized by XRD wide $\theta-2\theta$ scans in the 30°–100° range. Figure 2(a) shows the XRD spectra of AlN films deposited for 1 h at a working gas (pure nitrogen) pressure of 0.4–1.4 Pa, substrate temperature of 350 °C, and rf power of 400 W. All the specimens featured a single hexagonal AlN(002)

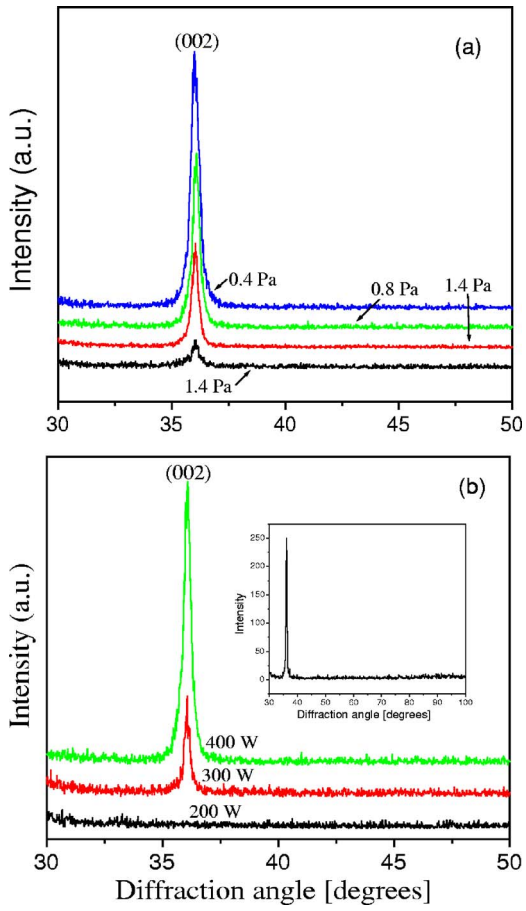

FIG. 2. (Color online) X-ray diffraction spectra of AlN films for different working gas pressures at a rf power of 400 W (a) and different rf powers at a pure nitrogen pressure of 0.8 Pa (b). In both cases the substrate temperature is 350 °C. The inset in panel (b) displays the XRD wide scan at a rf power of 400 W and the same other parameters as in case (b).

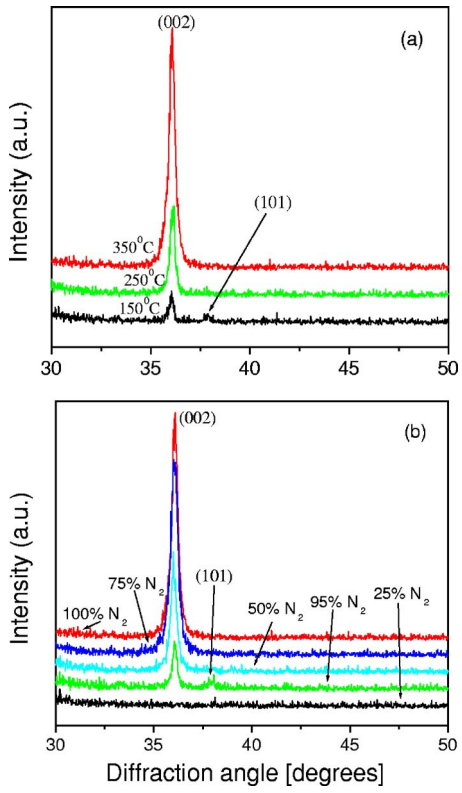

FIG. 3. (Color online) Same as in Fig. 2 for different substrate temperatures in pure nitrogen (a) and different N_2 concentrations at a surface temperature of 350 °C (b). In both cases, the rf power and working gas pressure are 400 W and 0.8 Pa, respectively.

peak at 36.1°.[4] The full width at half maximum (FWHM) of the AlN(002) peak has shown a strong dependence on the working gas pressure. The FWHM was calculated by using a Lorentz curve fit of the experimental data at 2θ between 34° and 38°. In the range of working gas pressures 0.4–1 Pa, the FWHM consistently decreased. At higher pressures (up to 1.4 Pa), the AlN(002) peak widened quite significantly. The FWHM has a clearly resolved minimum when the pressure is 0.8–1.1 Pa, which is indicative of somewhat better crystallization of the AlN films in this pressure range. To ascertain which working gas pressure p_0 yields a better c-axis (002) orientation, we also ran the XRD rocking curve measurements at θ=18.05°. This analysis has revealed that a sputtering pressure of 0.8 Pa leads to a smaller FWHM of 10.4° as compared to 18.6° at 1.1 Pa. Thus, the alignment of the growth direction [with respect to the (111) crystallographic direction of the silicon substrate] is improved in films synthesized at p_0=0.8 Pa. We thus conclude that the optimal sputtering pressure for the growth of highly c-axis oriented AlN films is 0.8 Pa.

Figure 2(b) shows the XRD patterns of the samples after 1 h deposition in pure nitrogen at a rf power of 200–400 W, substrate temperature of 350 °C, and sputtering pressure of 0.8 Pa. Interestingly, the film deposited at 200 W did not show any crystalline orientation peculiar to AlN. This may be attributed to the fact that when the rf power is low, the adatoms cannot gain enough energy to form crystalline structures on the substrate. However, a pronounced diffraction peak corresponding to the (002) plane appears when the input power is increased to 300 W. The (002) preferred orientation of AlN further improves at higher rf powers, as can be seen in Fig. 2(b).

Figure 3(a) shows the XRD spectra of the AlN films deposited in a 60 min process in pure nitrogen at the substrate temperature T_s=150–350 °C, gas pressure 0.8 Pa, and rf power P_{rf}=400 W. One can clearly see that the c axis remains the preferred growth direction within the entire temperature range considered. This growth direction becomes pronounced at substrate temperatures as low as 150 °C. At this temperature, there is also a weak reflection signal from the (101) crystalline plane seen in the XRD spectrum in Fig. 3(a).

The effect of variation of N_2 partial pressure relative to that of argon on XRD spectra of AlN films is shown in Fig. 3(b), where the partial pressure of N_2 (25%–100%) is shown as a percentage of the total pressure of the N_2+Ar gas mixture. The other process parameters are: p_0=0.8 Pa, P_{rf} =400 W, T_s=350 °C, and deposition time τ_D=60 min. One can notice that the specimens synthesized at 25% N_2 concentration did not show any crystalline AlN phase in the films. When the partial pressure of N_2 was very high (95% N_2 and only 5% Ar), there were two, (002) and (101) crystalline peaks, with the former being much stronger than the latter one. When nitrogen concentration was 75% and 100%, the

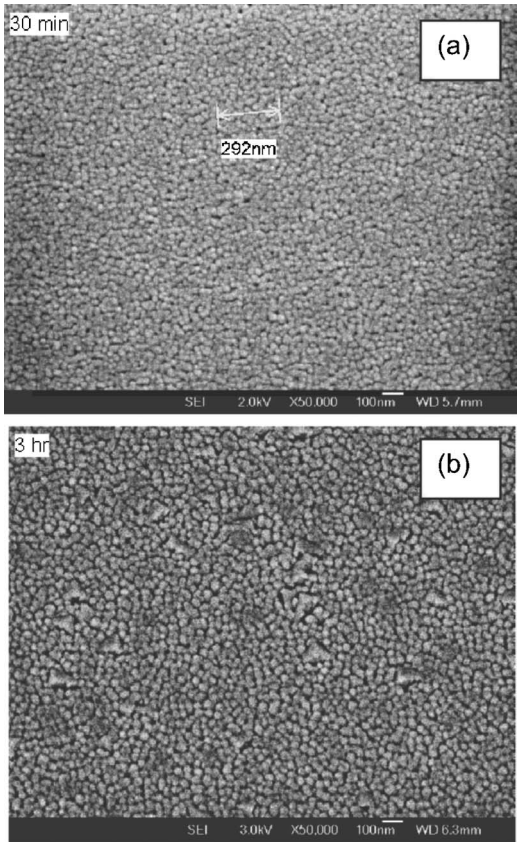

FIG. 4. Surface morphology of the AlN thin films deposited for 0.5 (a) and 3 h (b) imaged by field emission SEM. Optimized process conditions.

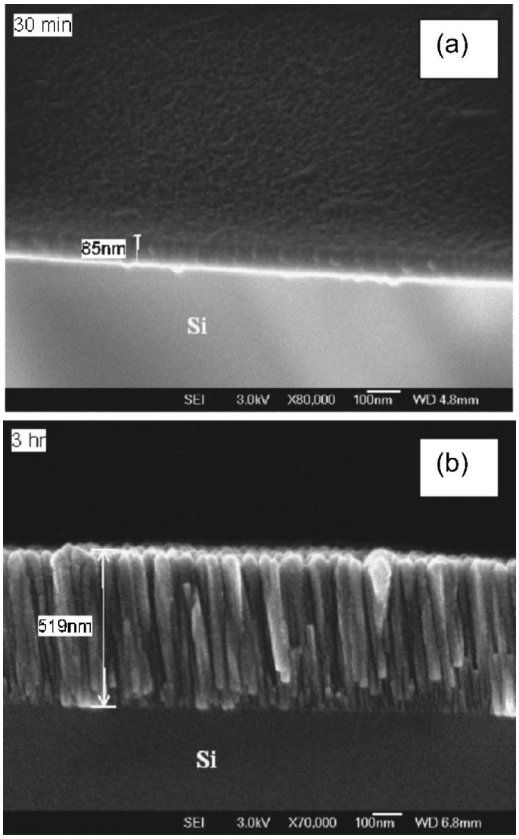

FIG. 5. Cross-sectional SEM micrograph of the AlN films deposited for 0.5 (a) and 3 h (b) and the same process conditions as in Fig. 4.

(002) peak intensity was significantly enhanced. Moreover, it was the only crystalline peak in the entire spectrum as was confirmed by the results of the wide XRD scans similar to those shown in the inset in Fig. 2(b).

In general, the (002) crystallographic orientation has always been the preferential growth direction when the partial pressure of nitrogen p_{N_2} exceeded a half of the total pressure of the $Ar+N_2$ gas mixture. Thus, as Fig. 3(b) suggests, the crystalline orientation is influenced by the relative partial pressures of nitrogen and argon gases. Nonetheless, at p_{N_2}/p_0 ratios larger than 0.5, the films appear perfectly oriented along the *c* axis. Therefore, the results of the XRD analyses show that the growth of highly oriented nanocrystalline AlN(002) thin film can be optimized at a sputtering pressure of 0.8 Pa, rf power of 400 W, substrate temperature of 350 °C, and relative ratio of partial pressures of N_2 and Ar gases 3:1 (75% concentration of N_2).

The top-view microstructure of platinum sputter-coated AlN films deposited for 0.5 and 3 h under the earlier optimized process conditions is depicted in Figs. 4(a) and 4(b), respectively. The surface morphology features smooth and homogeneously uniform pebble-like nanocrystalline grains (with a typical size within the 40–80 nm range) formed on the substrate with some larger (>100 nm) triangular-shaped particles on top of the layer; the latter appearing in the 3 h deposition process. The SEM images also reveal clear grain boundaries and also voids between the crystals. This compact and almost void-free crystalline structure (viewed from the top) is indicative of preferential columnar growth, which has been confirmed by the cross-sectional scanning electron microscopy. The cross-sectional SEM images of the AlN film grown for 0.5 and 3 h are shown in Figs. 5(a) and 5(b), respectively. From Fig. 5(a) one can also notice a thin (a few nanometers thick) amorphous layer along the interface between the AlN film and the Si(111) substrate. The film grown in the 3-h long process is approximately 0.5 μm thick and shows excellent vertical alignment of the columnar structure, which is quite similar to that of typical quasi-one-dimensional quantum confinement structures.[20,21]

The properties of such columnar structures could be attributed to the *Zone 1* structure.[28] In this model, tapered units defined by voided growth boundaries are superimposed on a microstructure that is usually amorphous at low temperatures. The voided growth defects that define the Zone 1 structure are a consequence of atomic shadowing. Shadowing induces open boundaries because high points on the growing surface receive a higher flux of plasma sputtered building units than the valleys, particularly when a significant oblique component is present in the flux (which is the case in our experiments; see the representative trajectories of sputtered species in Fig. 1). A typical aspect ratio of the highly oriented crystalline columnar structures was found in the range 7–15.

It is important to note that in plasma-based nanofabrication, ion fluxes play a prominent role in the growth dynamics and reshaping of similar large-aspect-ratio nanostructures. In particular, as the structures grow predominantly in one direction (as is the case for the AlN films of our interest here)[29]

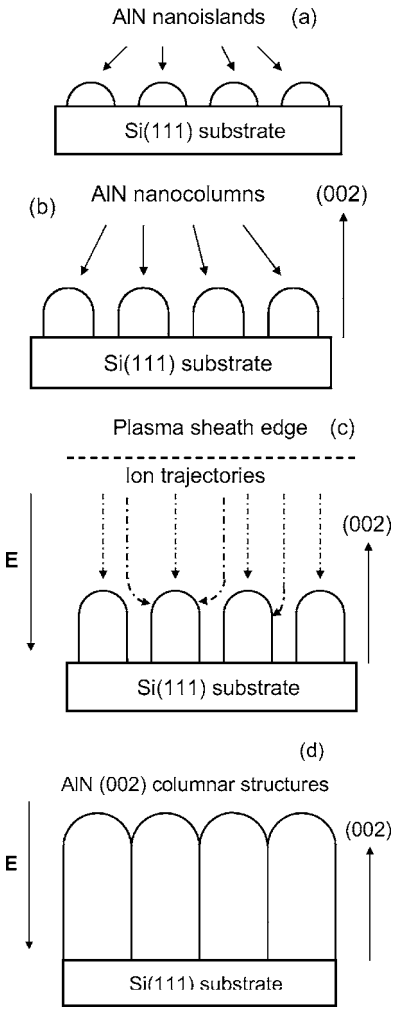

FIG. 6. Four main stages of the plasma/electric field-assisted growth of the AlN(002) columnar structures.

and elongate, ion fluxes from the plasma progressively focus onto sharper (near the top) sections of the growing nanostructures and contribute to further sharpening and elongation of the structures. This effect has previously been reported for plasma-assembled well-aligned gallium-doped zinc oxide nanorods.[31] Extensive numerical simulations also confirm the role of the plasma ions and electric fields in the growth, reshaping, and postprocessing (e.g., functionalization) of plasma-grown nanostructures of various dimensionality.[32–35]

In the case considered, during the initial growth stages, seed nuclei are formed and evolve into three-dimensional nanoislands on the surface, as sketched in Fig. 6(a). Initially, the shape of such growth islands can be close to spherical and they can develop as AlN nanodot patterns on Si(111) surface. When new growth slices are deposited onto a growing crystal surface, (002) emerges as the preferential growth direction,[36] which becomes even more energetically favorable under the action of the electric field in the plasma sheath; this gives rise to AlN nanocolumns depicted in Fig. 6(b). As the nanocolumns elongate, they focus ion fluxes toward their top sections; the AlN nanocolumns continue their growth along the direction of the electric field at a faster rate [Fig. 6(c)]. Despite a faster growth in the (002) crystallographic direction, the nanocones also widen, and overlapping AlN columnar structures depicted in Fig. 6(d), eventually emerge.

Thus, the plasma environment (i) contributes to the initial alignment of the nanocolumns; (ii) by affecting the attachment energies to different crystal facets (e.g., by increasing the surface temperature via ion bombardment and delivering higher-energy ionic building units to the growth slices), facilitates the thermokinetic selection of the (002) direction as the preferential growth direction; and (iii) plasma-generated ion fluxes focus onto top sections of the nanocolumns and increase the nanostructure growth rates.

The composition and chemical states in the as-grown samples have been analyzed by the XPS. Before the measurement, a 2 keV Ar^+ beam was used to sputter the film *in situ* to remove adventitious contaminants from the surface. The percentage atomic concentrations of elements in the film have been calculated by using the transmission functions and sensitivity factors for each of the constituent elements. Typically, the percentage atomic concentrations of Al and N were quite close to each other. There were also some traces of oxygen and carbon found. However, the abundance of O and C was typically one order of magnitude lower than that of the main constituent elements Al and N. This contamination is very difficult to eliminate completely and much higher concentrations of oxygen (owing to its large affinity to aluminum) have been reported by other authors.[3,39] Some oxygen is usually dissolved in the AlN lattice, while the remainder forms a thin amorphous oxide (Al_2O_3) coating on the surface of each AlN crystal.

Figures 7(a) and 7(b) show the narrow scan XPS spectra of Al $2p$ and N $1s$, respectively. The binding energy (BE) of the Al $2p$ photoelectron peak in Fig. 7(a) is 73.9 eV, and is attributed to the Al–N bonds in AlN.[40] The peak corresponding to Al–Al bonding (with the BE ~72 eV) was not detected in the Al $2p$ spectrum in Fig. 7(a). This suggests that all of the Al atoms are bonded with other elements and no metallic Al is present in the film. The N $1s$ spectrum in Fig. 7(b) was deconvoluted into the Gaussian/Lorentz peaks via the nonlinear least-squares routine yielding two peaks with binding energies of 397.3 and 399.3 eV. The strongest peak at 397.3 eV is characteristic of the N $1s$ state in the N–Al bond.[39] The almost negligible peak at 399.3 eV can be assigned to physisorbed molecular nitrogen, a common artifact of the sputter cleaning.

The elemental composition of the AlN films was further investigated by using EDX spectroscopy, which also took into account the presence of the Si(111) substrate due to a deeper penetration of the electron beam into the sample. The amplitudes of the elemental peaks were used to determine the relative intensities/percentage composition of each of the elements in the films. One of the most important observations was an increase of the nitrogen content with rf power, becoming optimum at P_{rf}=400 W. Interestingly, at P_{rf} =200 W, the nitrogen content was too low to form crystalline AlN films, which is cross referenced by the results of the XRD analysis in Fig. 2(b). Meanwhile, the level of oxygen presence in the films saturated when the rf power was increased. More importantly, the EDX analysis enabled us to

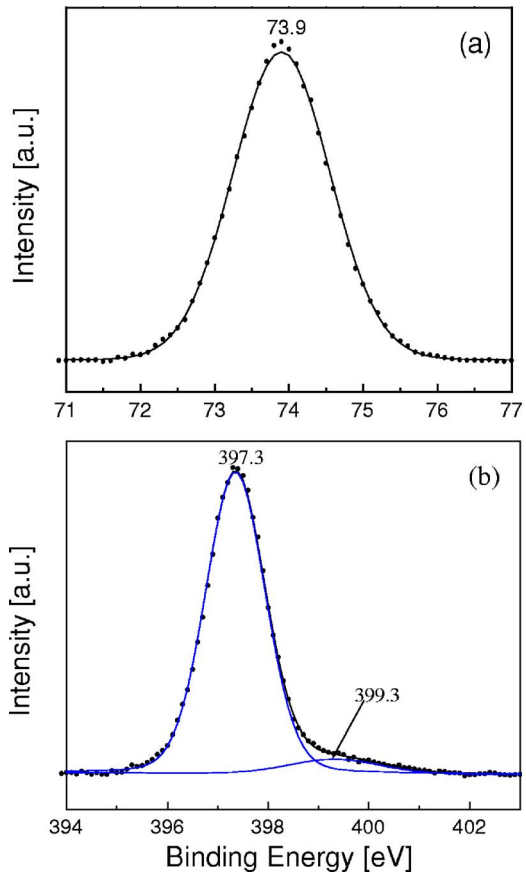

FIG. 7. (Color online) XPS narrow scan spectra of Al $2p$ (a) and N $1s$ (b) recorded from the AlN film deposited for 3 h.

elucidate the process conditions favorable for the synthesis of high-purity stoichiometric AlN. The normalized ratio of the EDX intensities of nitrogen and aluminum versus rf power is plotted in Fig. 8. Figure 8 suggests that an increase of the input power from 200 to 300 W leads to a drastic improvement in the [N]/[A] ratio toward 1. Thus, near-stoichiometric and highly oriented AlN films have been synthesized at a relatively high rf power level of 400 W.

The bonding states of AlN were further studied by means of Raman and FTIR spectroscopy. An incident beam at 514.5 nm was focused onto an area of $1-2$ μm in diameter to obtain the Raman spectra. Figure 9 shows the influence of the sputtering pressure on the phonon modes in the AlN films deposited in pure nitrogen ambient for 1 h at a rf power of 400 W, substrate temperature of 350 °C. The Raman spectra in Fig. 9 suggest that the AlN thin film is formed in the pressure range between 0.8 and 1.1 Pa, as suggested by clearly resolved characteristic AlN phonon modes at 657 cm^{-1} ($E2$ high) and 910 cm^{-1} [$E1$ longitudinal optical (LO)].[1] Phonon peaks at 615, 667, and 825 cm^{-1} are due to the silicon substrate[11] and are denoted by asterisks in Fig. 9. We have also studied the effect of the variation of the deposition time τ_D from 0.5 to 3 h on the Raman spectra of the films synthesized at a sputtering pressure of 0.8 Pa, rf power of 400 W, substrate temperature of 350 °C and 75% N_2 concentration. As the AlN film thickness increased, the $E2$ (high) phonon mode narrowed and became more distinct. Besides, the peak at 855 cm^{-1} due to the A_1 LO phonon mode appeared in the Raman spectra of thicker films, which further confirms the formation of the AlN. This is quite expected as the results of the Raman spectroscopy become more accurate for relatively thicker films. To reinforce the conclusions drawn form the Raman spectroscopy, a complementary FTIR analysis was performed at different rf powers and partial pressures of working gases.

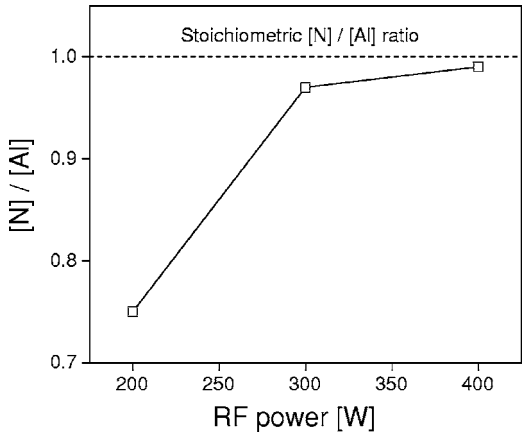

FIG. 8. Elemental ratio [N]/[Al] versus rf power. At rf powers exceeding 300 W, the [N]/[Al] ratio approaches the stoichiometric ratio 1:1.

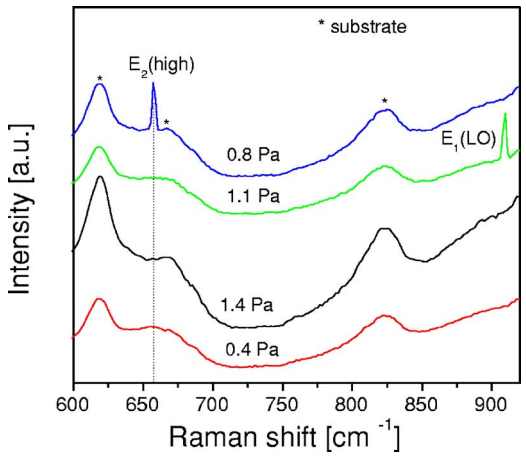

FIG. 9. (Color online) Raman spectra of AlN films at different working gas pressures in the range 0.4–1.4 Pa.

Figure 10 shows the infrared spectra of AlN films synthesized in a 60-min nitrogen plasma-based process at p_0 = 0.8 Pa, T_s = 350 °C, and rf powers 200–400 W. The peak at 682 cm^{-1} corresponds to the $E1$ transverse optical (TO) vibration mode of the infrared-active Al–N bond.[1] The peak is broad and shifted from its characteristic value of 670 cm^{-1} due to residual stresses.[4] Weaker peaks near 610 and 660 cm^{-1} are due to the Al–O stretching and O–Al–O bending modes, respectively,[41] indicating the presence of the aluminum oxide (Al_2O_3). This oxide component appears to be amorphous,[41] which is further supported by the absence in the XRD spectra of any peaks other than the (002) peak of highly oriented AlN. The broadband observed around 1110 cm^{-1} is most probably due to the asymmetric stretching mode of an oxygen atom in the Si–O–Si chain of amorphous silicon dioxide (a-SiO_2).[41] Interestingly, at a rf power of 200 W, the $E1$ (TO) AlN phonon mode was absent and the vibra-

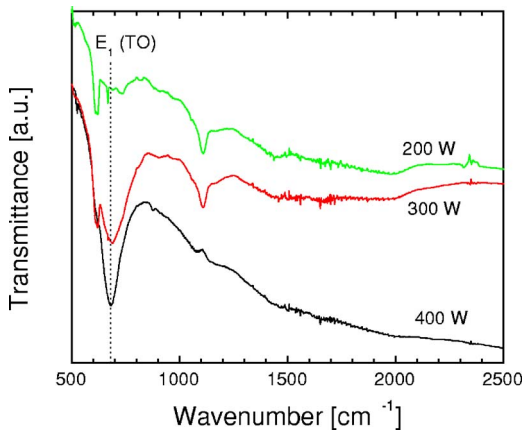

FIG. 10. (Color online) Infrared transmittance of AlN films at 0.8 Pa nitrogen gas pressure, substrate temperature 350 °C, and different rf power.

tions due to the SiO_2 were prominent. Also, the $E1$ (TO) linewidth narrowed as the power increased indicating a better quality of the AlN films synthesized at higher rf powers. This is consistent with the results obtained from the XRD spectra at different rf powers [Fig. 2(b)], which suggest that no crystalline AlN film have been formed at $P_{rf}=200$ W and that a further increase in the intensity of the (002) peak is proportional to the input power. The FTIR results also suggest that when the partial pressure of nitrogen was less than a half of the total gas pressure ($p_{N_2}/p_0<0.5$), no phonon modes characteristic to AlN were detected. Furthermore, the FWHM of the peak related to the $E1$ (TO) phonon mode was noticeably larger in pure nitrogen compared to the case when $p_{N_2}/p_0=0.75$. Thus, the film quality was better when the relative percentage of N_2 was 75%, which further justifies our choice of the optimum process conditions.

The AlN films deposited on glass substrates were also investigated for their optical properties. The optical transmittance spectrum of an AlN film deposited for an hour under the optimal growth conditions is shown in Fig. 11 (dotted line). Reference transmittance of uncoated glass substrates is also shown in Fig. 11 by a solid line. A comparison of the spectral characteristics of the glass and AlN-coated glass

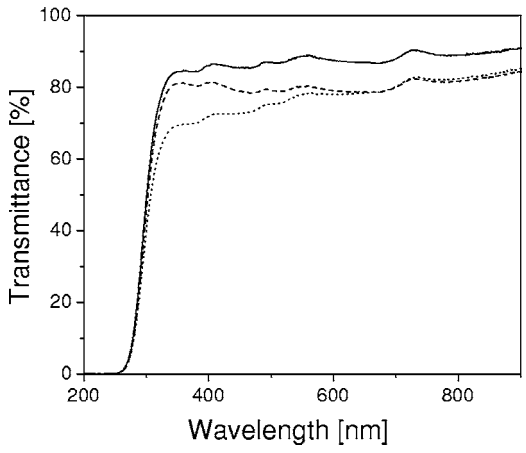

FIG. 11. Optical transmittance spectrum of AlN film deposited for 1 h on glass substrates. The solid line is for the glass reference sample and the dashed and dotted lines are for AlN films synthesized from $Ar+N_2+H_2$ and $Ar+N_2$ gas mixtures, respectively.

specimens suggests that the AlN film has a lower transmittance of ~8%–14% (compared to the glass substrate) in the visible region (400–780 nm) of the spectrum. The main cause of incident light loss is due to surface reflection whereas a very small amount of light is absorbed. The onset of the band edge and interband absorption results in a reduced transmittance of the AlN sample. Since optical coatings are required to be visible in the whole of the visible spectrum, this feature is undesirable from the optical applications point of view.

In order to improve the optical transmittance of the AlN films of our interest here, the samples were also synthesized by introducing a small percentage (~5%) of H_2 gas to the $Ar+N_2$ gas mixture. The addition of hydrogen results in the growth of AlN:H (hydrogenated AlN) films which, unlike the AlN films, exhibited a better transparency in the 300–600 nm spectral range (dashed line in Fig. 11). In this case, there is a significant reduction in the near-band-edge absorption.[42] This kind of behavior can be explained in terms of the reduced density of states at the band edges of the crystalline AlN material as a consequence of the passivation of the dangling bonds due to the addition of hydrogen in the films.

IV. CONCLUSION

Optically transparent, highly oriented (002) nanocrystalline AlN films have been successfully synthesized using the $Ar+N_2$ plasma-assisted rf magnetron sputtering of aluminum at a low temperature of 350 °C. The results of the XRD analysis indicate that single-crystalline and highly oriented AlN films are formed at a sputtering pressure of 0.8 Pa, rf power of 400 W, and relative partial pressure of nitrogen in the $Ar+N_2$ mixture of 75%. SEM cross-sectional micrographs show that the films feature a columnar structure overcoated by a thin (a few nanometers thick) amorphous layer. The XPS and EDX analyses suggest that the films of our interest here contain chemically pure and near-stoichiometric AlN. FTIR and Raman spectroscopy results confirm the presence of strong Al–N bonding in the films. Moreover, the AlN(200) films exhibit an excellent optical transmittance of ~80% to visible light, making it also promising for optical applications.

ACKNOWLEDGMENTS

This work was partially supported by the Agency for Science, Technology and Research (Singapore), the Australian Research Council, the University of Sydney, and the International Research Network for Deterministic Plasma-Aided Nanofabrication. The assistance of J. W. Chai in the XPS analysis is kindly appreciated.

[1]M. Kuball, Surf. Interface Anal. **31**, 987 (2001).
[2]S. C. Jain, M. Willander, J. Narayan, and R. Van Overstraeten, J. Appl. Phys. **87**, 965 (2000).
[3]H. Morkoc, *Nitride Semiconductors and Devices* (Springer, New York, 1999).
[4]G. W. Auner, F. Jin, V. M. Naik, and R. Naik, J. Appl. Phys. **85**, 7879 (1999).
[5]V. Ligatchev, Rusli, and Z. Pan, Appl. Phys. Lett. **87**, 242903 (2005).
[6]A. R. Goni, H. Siegle, K. Syassen, C. Thomsen, and J.-M. Wagner, Phys. Rev. B **64**, 035205 (2001).

[7]A. L. Alvarez *et al.*, J. Appl. Phys. **92**, 223 (2002).
[8]A. Sarua, M. Kuball, and J. E. Van Nostrand, Appl. Phys. Lett. **81**, 1426 (2002).
[9]T. Prokofyeva, M. Seon, J. Vanbuskirk, M. Holtz, S. A. Nikishin, N. N. Faleev, H. Temkin, and S. Zollner, Phys. Rev. B **63**, 125313 (2001).
[10]H. Harris, N. Biswas, H. Temkin, S. Gangopadhyay, and M. Strathman, J. Appl. Phys. **90**, 5825 (2001).
[11]C. T. M. Ribeiro, F. Alvarez, and A. R. Zanatta, Appl. Phys. Lett. **81**, 1005 (2002).
[12]R. S. Naik, R. Reif, J. J. Lutsky, and C. G. Sodini, J. Electrochem. Soc. **146**, 691 (1999).
[13]R. D. Vispute, J. Narayan, H. Wu, and K. Jagannadham, J. Appl. Phys. **77**, 4724 (1995).
[14]S. Y. Huang, S. Xu, J. D. Long, Z. Sun, and T. Chen, Phys. Plasmas **13**, 023506 (2006).
[15]S. Y. Huang *et al.*, Physica E (Amsterdam) **31**, 200 (2006).
[16]V. M. Ng, M. Xu, S. Y. Huang, J. D. Long, and S. Xu, Thin Solid Films **506–507**, 283 (2006).
[17]Z. L. Tsakadze, K. Ostrikov, J. D. Long, and S. Xu, Diamond Relat. Mater. **13**, 1923 (2004).
[18]Z. L. Tsakadze, K. Ostrikov, and S. Xu, Surf. Coat. Technol. **191**, 49 (2005).
[19]S. Xu, K. Ostrikov, J. D. Long, and S. Y. Huang, Vacuum **80**, 621 (2006).
[20]K. Ostrikov, Rev. Mod. Phys. **77**, 489 (2005).
[21]K. Ostrikov, J. D. Long, P. P. Rytkevych, and S. Xu, Vacuum **80**, 1126 (2006); S. V. Vladimirov and K. Ostrikov, Phys. Repts **393**, 175 (2004).
[22]S. Xu, J. D. Long, L. Sim, C. H. Diong, and K. Ostrikov, Plasma Processes Polym. **2**, 373 (2005); W. Zhou *et al.*, Surf. Coat. Technol. **200**, 6155 (2006).
[23]N. Jiang, S. Xu, K. N. Ostrikov, J. Chai, Y. Li, M. L. Koh, and S. Lee, Thin Solid Films **385**, 132 (2001).
[24]S. K. Ghandhi, *VLSI Fabrication Principles*, 2nd ed. (Wiley, New York, 1994).
[25]S. Xu, K. Ostrikov, Y. A. Li, E. L. Tsakadze, and I. R. Jones, Phys. Plasmas **8**, 2549 (2001).
[26]K. N. Ostrikov, S. Xu, and A. B. M. Shafiul Azam, J. Vac. Sci. Technol. A **20**, 251 (2002).
[27]I. B. Denysenko, S. Xu, P. P. Rutkevych, J. D. Long, N. A. Azarenkov, and K. Ostrikov, J. Appl. Phys. **95**, 2713 (2004).
[28]J. A. Thornton, J. Vac. Sci. Technol. A **4**, 3059 (1986).
[29]On plasma-exposed surfaces, many common high-aspect-ratio nanostructures (e.g., nanotubes or nanorods) are aligned vertically; this predominant growth direction is usually the same as the direction of the electric field in the near-substrate plasma sheath. If no external electric field is applied, the electric field is normal to the surface, which results in a vertical alignment of such nanostructures along the normal to the substrate surface. However, the alignment of the nanostructure growth can be controlled by external electric fields. For instance, in this way carbon nanotubes can be bent in sharp, pre-determined angles (e.g., 90°) to form L-shaped nanotubes (see Ref. 30).
[30]J. F. AuBuchon, L.-H. Chen, and S. Jin, J. Phys. Chem. B **109**, 6044 (2005).
[31]M. Yan, H. T. Zhang, E. J. Widjaja, and R. P. H. Chang, J. Appl. Phys. **94**, 5240 (2003).
[32]I. Levchenko, K. Ostrikov, M. Keidar, and S. Xu, Appl. Phys. Lett. **89**, 033109 (2006).
[33]I. Levchenko, K. Ostrikov, M. Keidar, and S. Xu, J. Appl. Phys. **98**, 064304 (2005).
[34]E. Tam, I. Levchenko, and K. Ostrikov, J. Appl. Phys. **100**, 036104 (2006).
[35]I. Levchenko, K. Ostrikov, and E. Tam, Appl. Phys. Lett. **89**, 223108 (2006).
[36]The preferential growth direction is usually determined by analyzing specific values of the attachment energy $E_{att}=E_{latt}-E_{slice}$, of the growth slice with the energy E_{slice} to the growing crystal with the lattice energy E_{latt}. The growth rate of a particular crystal facet is controlled by the attachment energy E_{att} (see Refs. 37 and 38).
[37]Z. Berkovitch-Yellin, J. Am. Chem. Soc. **107**, 8239 (1985).
[38]R. Docherty, G. Clydesdale, K. J. Roberts, and P. Bennema, J. Phys. D **24**, 89 (1991).
[39]N. Laidani, L. Vanzetti, M. Anderle, A. Basillais, C. Boulmer-Leborgne, and J. Perriere, Surf. Coat. Technol. **122**, 242 (1999).
[40]J. F. Moulder, W. F. Stickle, P. E. Sobol, and K. D. Bomben, *Handbook of X-Ray Photoelectron Spectroscopy* (Physical Electronics, Inc., Minneapolis, 1995).
[41]A. R. Chowdhuri, C. G. Takoudis, R. F. Klie, and N. D. Browning, Appl. Phys. Lett. **80**, 4241 (2002).
[42]N. F. Mott and E. A. Davis, *Electronic Processes in Nonccrystalline Solids* (Clarendon, Oxford, 1979).